Flat Spin of Axisymmetric Bodies in the Critical Reynolds Number Region

L. E. Ericsson*
Lockheed Missiles & Space Company, Sunnyvale, California

An analysis of experimental results from tests of bodies with circular cross section shows the flat-spin motion, which only occurs in the critical Reynolds number region, to be caused primarily by the moving-wall effect generated by the translating body surface. This effect is balanced by the effect of the spin-induced change of the local, external flow environment, resulting in a steady flat-spin motion. The analysis provides a simple analytical method for prediction of the maximum flat-spin rate.

Nomenclature

d = cylinder diameter
D' = sectional drag; coefficient $c_d = D'/(\rho_\infty U_\infty^2/2)d$
k = roughness height
ℓ = sectional lift; coefficient $c_\ell = \ell/(\rho_\infty U_\infty^2/2)d$
l = body length
p = roll rate
P = pressure; coefficient $C_p = (P-P_\infty)/(\rho_\infty U_\infty^2/2)$
Re = Reynolds number $= U_\infty d/\nu_\infty$
S = reference area $= \pi d^2/4$
t = time
U = velocity
V = translatory velocity
x = distance from nose tip
Y = side force; coefficient $C_Y = Y/(\rho_\infty U_\infty^2/2)S$
α = angle of attack
ν = kinematic viscosity
ρ = air density
φ = meridional coordinate from the stagnation point on a stationary model (see Fig. 6)
ϕ = coning angle
Ω = flat-spin angular rate $= \partial\phi/\partial t$ for $\alpha = 90$ deg

Subscripts

AS = asymmetric separation
B = base
D = drag-induced
eff = effective
FS = flat spin
L = local
RC = rotation center
W = wall
∞ = freestream conditions

Introduction

THE interest in the flat-spin problem stems from the fact that when a slender body with the center of gravity at midbody, such as an empty strap-on booster, is dropped in the atmosphere, it develops a high-rate flat-spin motion, as has been demonstrated in drop tests.[1] Consequently, systematic experiments in a ground facility on a series of axisymmetric bodies of interest have been performed[1] (Fig. 1). The results compliment those obtained earlier,[2] and provide the basis for a follow-up of the analysis initiated in Ref. 3.

Static tests of an $l/d = 3.82$ circular cylinder[2] (Fig. 2a) showed a side force developing in the critical Reynolds number region where the asymmetric, one-bubble flow separation had been observed in two-dimensional (2D) tests[4] (Fig. 2b). If the asymmetry were the same across the span for the finite l/d cylinder,[2] as in the 2D test,[4] no yawing moment and, consequently, no flat spin would develop around a midbody rotation axis. The pressure measurements on a cylinder, driven at 500 rpm around the midbody axis, showed that the local rotation-induced effects produced the critical flow asymmetry in different directions on both sides of the rotation axis[2] (Fig. 3). As this generated a prospin yawing moment, it is clear how the observed steady-state flat spin was produced. At or near the critical Reynolds number, body and/or flow asymmetries could initiate an initial spin-producing moment. Once the initial spin direction had been determined, the spin-induced moving-wall effects took over.[3]

Moving-Wall Effect

The classical Magnus lift characteristics of a rotating circular cylinder represent a pure case of moving-wall effects.[5] Using the wall-jet-like effect of the moving wall, one can explain the observed Magnus lift characteristics in Ref. 5 as follows: The downstream moving wall delays flow separation

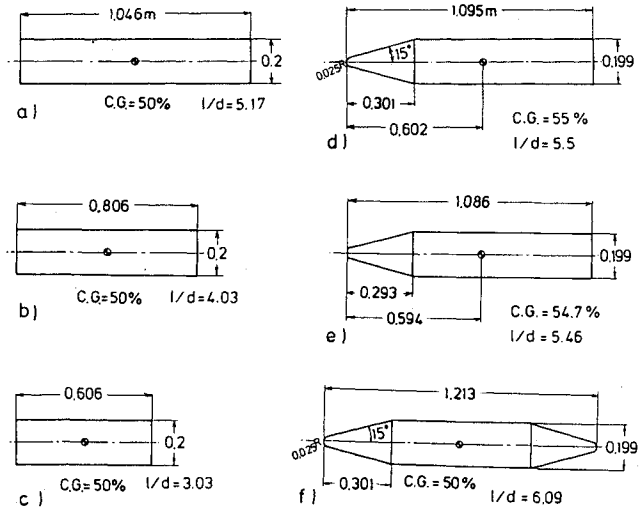

Fig. 1 Tested canister shapes.[1]

Received Aug. 7, 1986; presented as Paper 86-2083 at the AIAA Atmospheric Flight Mechanics Conference, Williamsburg, VA, Aug. 18-20, 1986; revision submitted Nov. 7, 1986.

*Senior Consulting Engineer. Fellow AIAA.

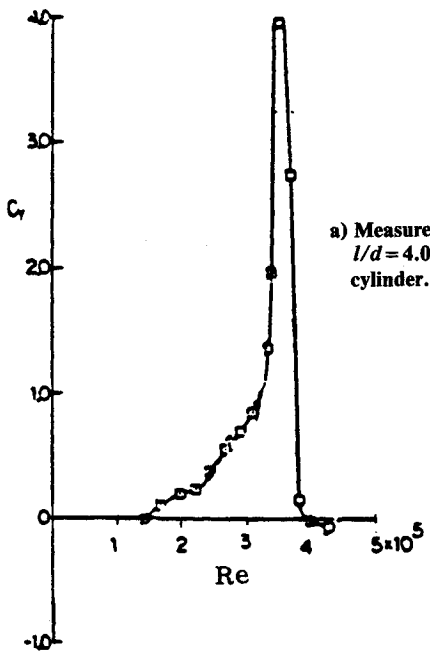

a) Measured side force on $l/d=4.03$ circular cylinder.[2]

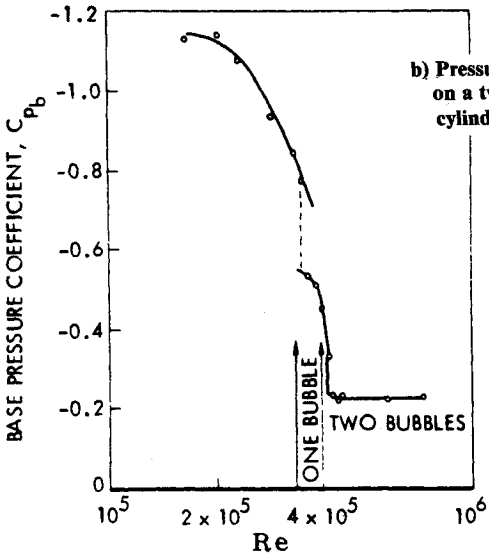

b) Pressure distribution on a two-dimensional cylinder.[4]

Fig. 2 Aerodynamic characteristics of a circular cylinder in the critical Reynolds number region.

and the upstream moving wall promotes separation (Fig. 4). For the subcritical, laminar (for zero spin rate, $U_W=0$) flow case in Fig. 4, the Magnus lift is generated mainly by the downstream moving-wall effect on the top side, moving the separation from the subcritical toward the supercritical position. On the bottom side, the separation is already of the subcritical type at $p=0$, and the upstream moving-wall effect does not have much leverage for its separation-promoting action. (The asymmetric flow separation is responsible for most of the lift generation.)

These moving-wall effects on flow separation are rather straightforward and explain the positive Magnus lift slopes, $\partial c_\ell/\partial(U_W/U_\infty)>0$. What about the negative slopes, $\partial c_\ell/\partial(U_W/U_\infty)<0$, occurring at a critical wall velocity? These so-called Magnus lift reversals are caused by the moving-wall effect on boundary-layer transition.[6] When $p>p_{crit}$, the upstream moving-wall effect on the bottom side causes boundary-layer transition to occur before separation, changing it from the subcritical to the supercritical type. This effect completely overpowers the regular moving-wall effects and causes a more or less discontinuous loss of lift (Fig. 4).

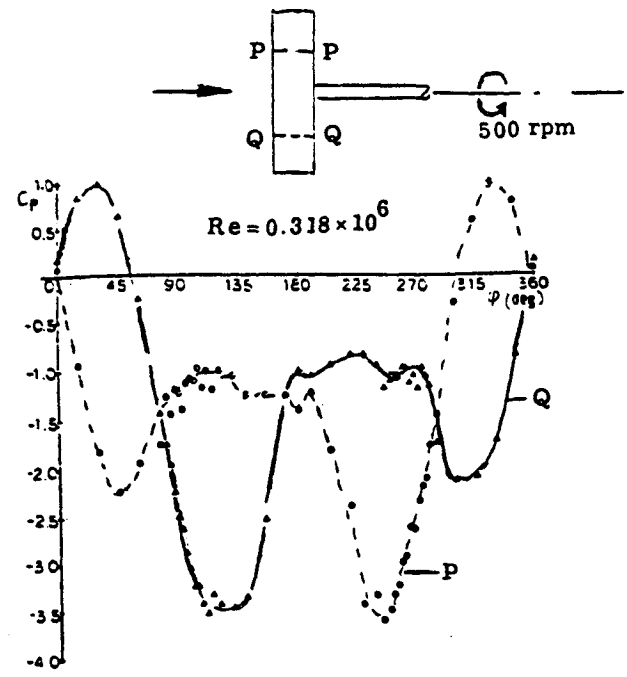

Fig. 3 Measured pressure distributions on a circular cylinder in flat spin.[2]

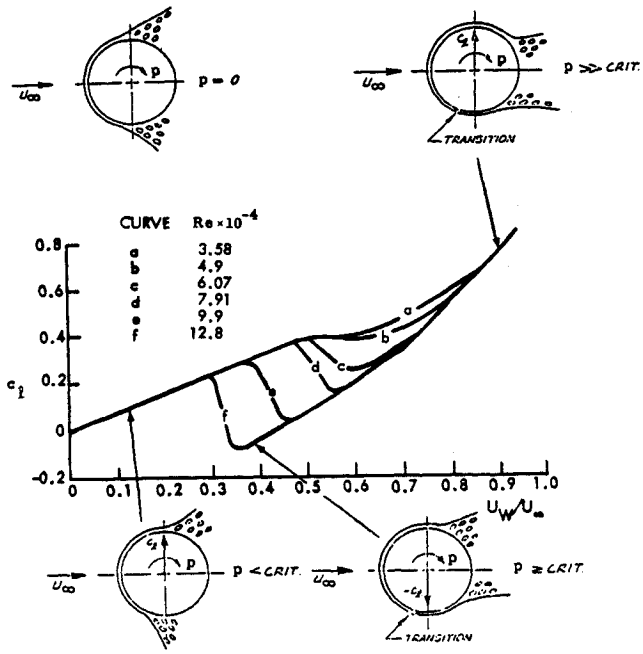

Fig. 4 Moving-wall effects on a circular cylinder in laminar flow.

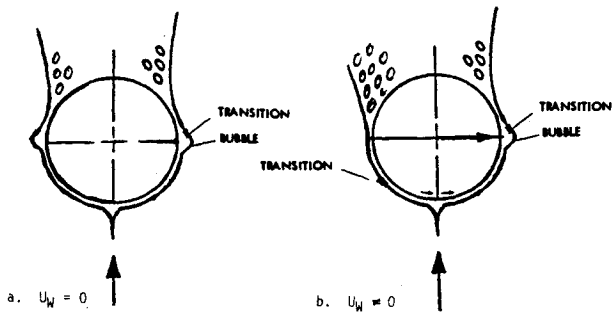

Fig. 5 Moving-wall effect on translating circular cross section in the critical Reynolds number region.

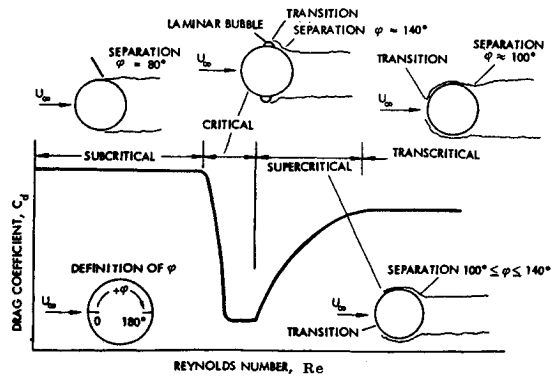

Fig. 6 Effect of Reynolds number on the drag of a circular cylinder.[9]

It is shown in Refs. 6 and 7 that the moving-wall effects are very similar for rotating and translating circular cross sections, because the dominant moving-wall effect occurs in the boundary-layer formation region between the stagnation and separation points. The main moving-wall effects on the boundary layer occur within the first 20-deg azimuth from the stagnation point.[8]

In the critical Reynolds number region, flow separation is complicated by the presence of a laminar separation bubble (Fig. 5a). The laminar flow separation develops near the lateral meridian ($\varphi = 90$ deg) and is followed by transition in the lifted shear layer, which causes flow reattachment. The reattaching turbulent boundary layer is able to withstand the adverse pressure gradient until $\varphi \approx 140$ deg before separation occurs. This is far aft of the separation location for a fully tur-

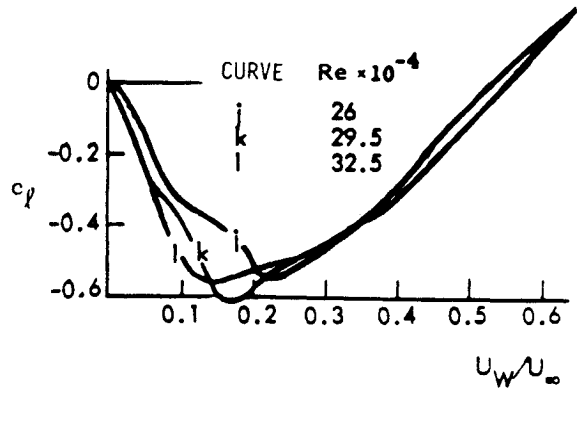

a) Lift coefficient.

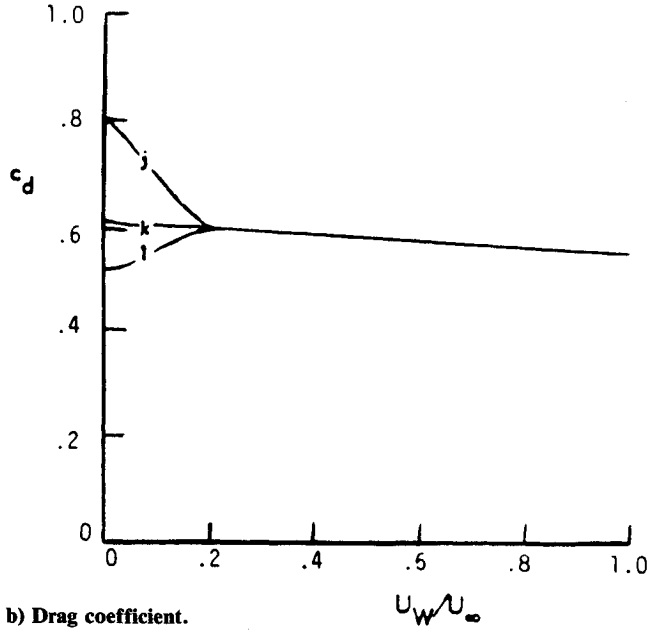

b) Drag coefficient.

Fig. 7 Moving-wall effects on a circular cross section in the critical Reynolds number region.[5]

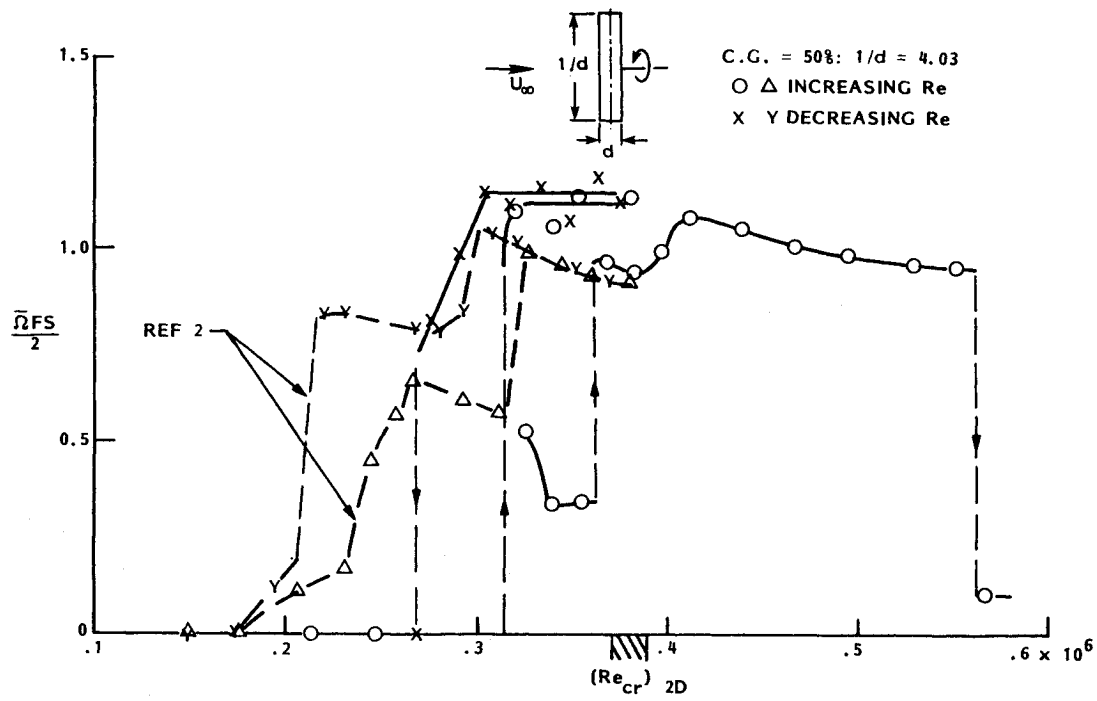

Fig. 8 Measured flat-spin rate on an $l/d = 4.03$ circular cylinder.[1]

bulent boundary layer, $\varphi \approx 100$ deg, resulting in a "drag bucket" for the critical Reynolds number region[9] (Fig. 6).

When the Reynolds number is increased, transition moves forward in the bubble shear layer. This generates a more fully turbulent flow profile in the reattaching shear layer, resulting in a delay of the final turbulent flow separation. This amplification of the beneficial effect of the increasing Reynolds number continues until transition reaches the top of the bubble, where it will remain until the Reynolds number has been increased enough to overcome the transition delay caused by local accelerated flow effects. The minimum drag plateau in Fig. 6 is probably the result of this momentary arrest of the forward transition movement with the increasing Reynolds number. When the Reynolds number is increased further, transition jumps forward of the bubble, wiping it out. The resulting super-critical type separation increases with the increasing Reynolds number and associated increased boundary-layer thickness, resulting in increased drag[9] (Fig. 6).

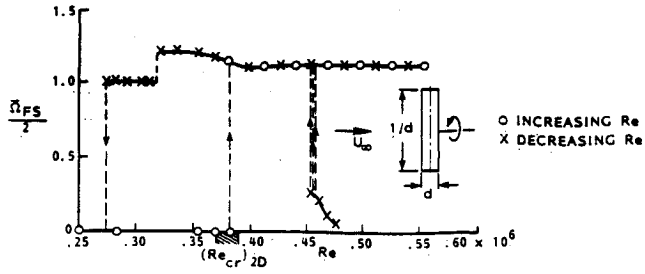

a) $l/d = 5.17$.

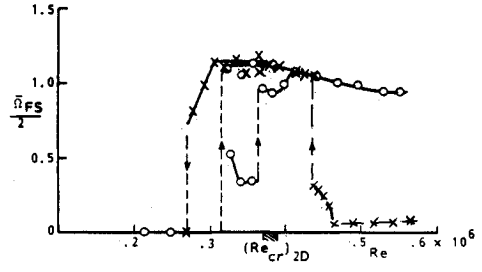

b) $l/d = 4.03$.

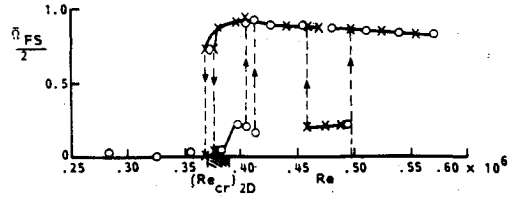

c) $l/d = 3.03$.

Fig. 9 Effect of "aspect ratio" l/d on flat-spin rate of a circular cylinder.[1]

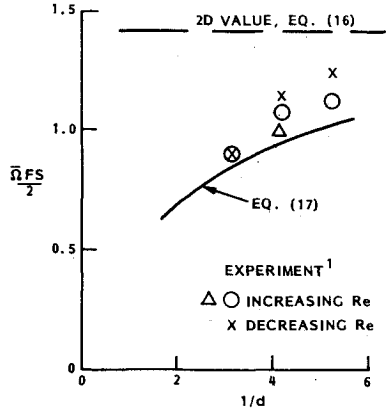

Fig. 10 Comparison between predicted and measured maximum flat-spin rate of circular cylinders.

In the case of a translating circular cross section (Fig. 5b), the upstream moving-wall effect will cause transition to occur upstream of the flow separation, exactly as in the case of the rotating cylinder (Fig. 4). The resulting movement of the final turbulent flow separation from $\varphi \approx 140$ deg toward $\varphi \approx 100$ deg results in a side force that will drive the translatory motion, thus explaining the experimentally observed flat spin in the critical Reynolds number region. To be able to predict the flat-spin rate would obviously be important for the design of axisymmetric containers to be air-dropped, especially if the content is sensitive to the spin-induced g loads. In what follows, a simple analysis, which provides the means for prediction of the maximum flat-spin rate, is performed.

Analysis

The spin-induced local velocity component as a fraction of freestream velocity is

$$\frac{V_L}{U_\infty} = \frac{(x - x_{RC})\Omega}{U_\infty} \tag{1}$$

The cross section translating at velocity V_L relative to the freestream velocity U_∞ has an effective total velocity:

$$V_{eff} = U_\infty \sqrt{1 + (V_L/U_\infty)^2} \tag{2}$$

V_{eff} is tilted relative to U_∞ an angle ϕ_V

$$\phi_V = \arctan(V_L/U_\infty) \tag{3}$$

The drag component counteracting the translatory motion is

$$\frac{\rho U_\infty^2}{2} S \left(\frac{\partial C_Y}{\partial x}\right)_D = -\frac{\rho V_{eff}^2}{2} S c_d \sin\phi_V \tag{4}$$

That is,

$$\left(\frac{\partial C_Y}{\partial x}\right)_D = -c_d \frac{V_L}{U_\infty} \sqrt{1 + \left(\frac{V_L}{U_\infty}\right)^2} \tag{5}$$

With (V_L/U_∞) from Eq. (1), one obtains Eq. (5) in the following form:

$$\left(\frac{\partial C_Y}{\partial \eta}\right)_D = -c_d \bar{\Omega} \eta \sqrt{1 + \bar{\Omega}^2 \eta^2} \tag{6}$$

$$\eta = (x - x_{RC})/l$$

$$^{\infty}\Omega/l\mho = \underline{\mho}$$

The cross-sectional load resulting from the separation asymmetry (Fig. 5b), which balances this damping load in the case of the final flat-spin state, is

$$\frac{\rho U_\infty}{2} S \left(\frac{\partial C_Y}{\partial x}\right)_{AS} = \frac{\rho V_{eff}^2}{2} S \Delta c_\ell \cos\phi_V \tag{7}$$

where Δc_ℓ is the negative Magnus lift.

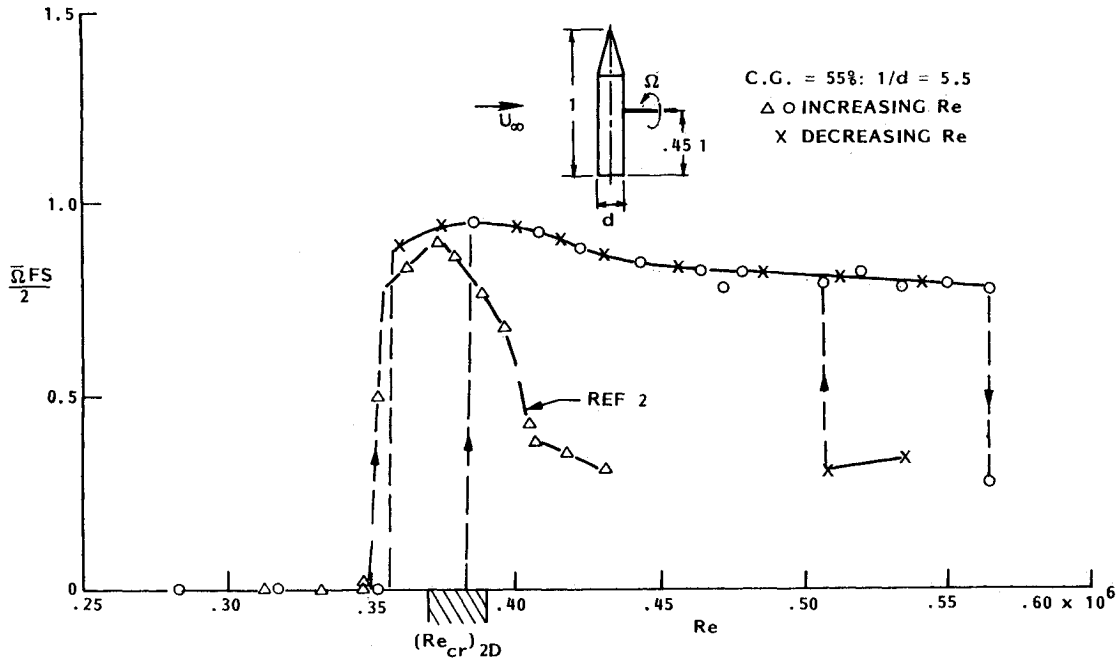

Fig. 11 Measured flat-spin rate of a cone-cylinder body.[1]

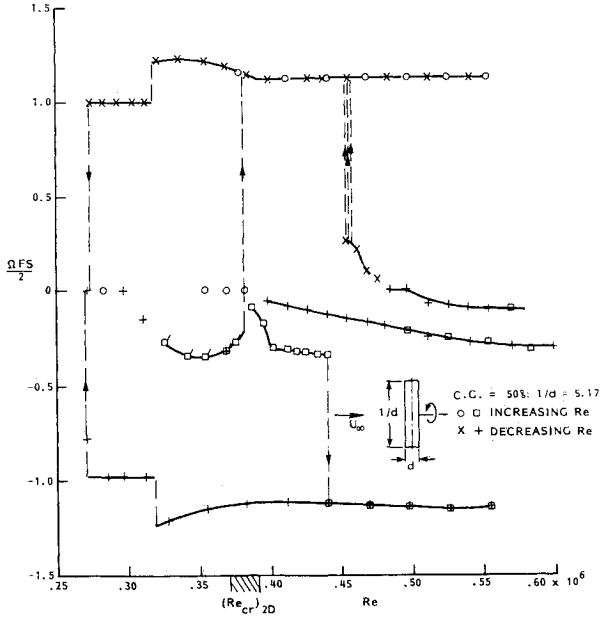

Fig. 12 Reynolds number hysteresis effects on flat-spin rate of an $l/d = 5.17$ circular cylinder.[1]

Combining Eqs. (1–3) and (7) gives

$$\left(\frac{\partial C_Y}{\partial x}\right)_{AS} = \Delta c_l \sqrt{1 + \bar{\Omega}^2 \eta^2} \tag{8}$$

Equation (8) is valid only for $\eta \geq 0$. For $\eta < 0$, Δc_ℓ changes sign, as is clear from earlier discussion.

Thus, one must write Eq. (8) in the following form:

$$\left(\frac{\partial C_Y}{\partial x}\right)_{AS} = \Delta c_l^* \sqrt{1 + \bar{\Omega}^2 \eta^2} \tag{9}$$

where

$$\Delta c_l^* = \Delta c_\ell, \quad \eta > 0$$
$$= -\Delta c_\ell, \quad \eta < 0$$

The condition for steady-state flat spin is

$$\int_{-x_{RC}/l}^{1-x_{RC}/l} \left[\left(\frac{\partial C_Y}{\partial x}\right)_D + \left(\frac{\partial C_Y}{\partial x}\right)_{AS}\right] \eta \, d\eta = 0 \tag{10}$$

Equations (6), (9), and (10) define the following steady-state spin rate:

$$\bar{\Omega}_{FS} = \int_{-x_{RC}/l}^{1-x_{RC}/l} \Delta c_l^* \sqrt{1 + \bar{\Omega}^2 \eta^2} \eta \, d\eta \Big/ \int_{-x_{RC}/l}^{1-x_{RC}/l} c_d \sqrt{1 + \bar{\Omega}^2 \eta^2} \eta^2 \, d\eta \tag{11}$$

For circular cylinders with large "aspect ratio" l/d, one can expect to get a reasonable result by assuming two-dimensional flow conditions, i.e., c_d and Δc_l^* remain constant. For low spin rates, $\bar{\Omega}^2 \ll 1$, Eq. (11) gives

$$\bar{\Omega}_{FS} \approx \frac{3}{2} \frac{\Delta c_l}{c_d} \left[\left(1 - \frac{x_{RC}}{l}\right)^2 + \left(\frac{x_{RC}}{l}\right)^2\right] \Big/ \left[\left(1 - \frac{x_{RC}}{l}\right)^3 + \left(\frac{x_{RC}}{l}\right)^3\right] \tag{12}$$

For high spin rates, $\bar{\Omega}^2 \gg 1$, one obtains

$$\bar{\Omega}_{FS} \approx \frac{4}{3} \frac{\Delta c_l}{c_d} \left[\left(1 - \frac{x_{RC}}{l}\right)^3 + \left(\frac{x_{RC}}{l}\right)^3\right] \Big/ \left[\left(1 - \frac{x_{RC}}{l}\right)^4 + \left(\frac{x_{RC}}{l}\right)^4\right] \tag{13}$$

For $x_{RC}/l = 0.5$, Eqs. (12) and (13) give

$$\frac{8}{3} \leq \bar{\Omega}_{FS} \Big/ \frac{\Delta c_l}{c_d} \leq \frac{9}{3} \tag{14}$$

That is, for finite $\bar{\Omega}_{FS}$, the flat-spin rate around $x_{RC}/l = 0.5$ can be approximated as

$$\bar{\Omega}_{FS} \approx \frac{17}{6} \frac{\Delta c_l}{c_d} \tag{15}$$

The maximum transition-induced asymmetry on a rotating cylinder[5] (Fig. 7a) gives a value of $\Delta c_\ell \approx 0.6$, and the corresponding drag value (Fig. 7b) is $c_d \approx 0.6$. That is, the two-dimensional $\Delta c_\ell / c_d$ value in Eq. (15) is roughly unity, giving

$$\bar{\Omega}_{FS} \approx 17/6 \tag{16}$$

According to Ref. 10, centrifugal and Coriolis forces are of negligible magnitude for the circular cylinder.

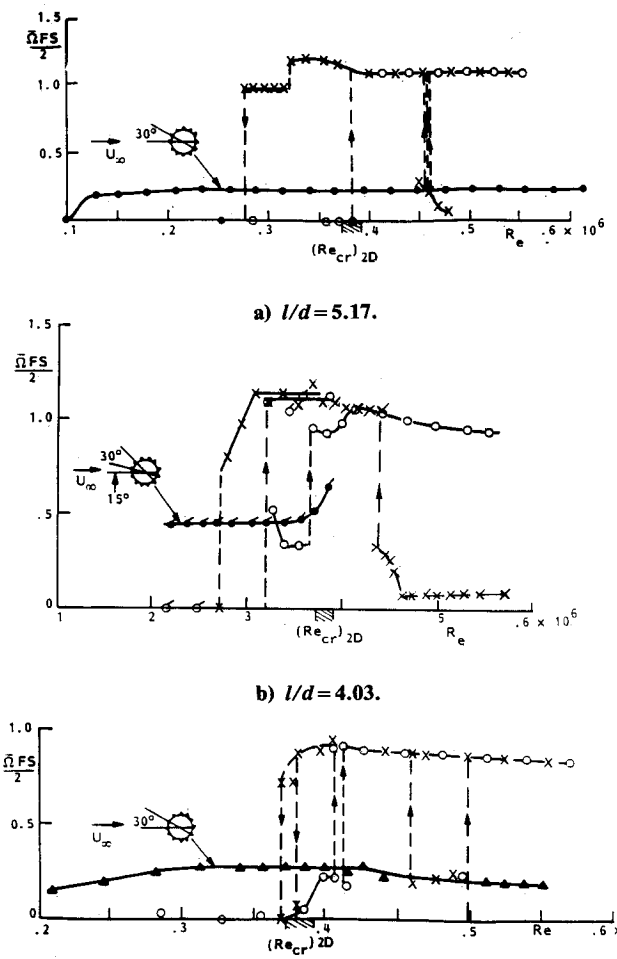

a) $l/d = 5.17$.

b) $l/d = 4.03$.

c) $l/d = 3.03$.

Fig. 13 Effect of boundary-layer trips on the flat-spin rate of circular cylinders.[1]

Discussion of Results

The experimental results[1] in Fig. 8 show that the prediction by Eq. (16) overestimates the maximum flat-spin rate. (The ordinate $\bar{\Omega}_{FS}/2$ is used to present the results as was done in Ref. 1, which is in agreement with common usage.) As expected, the predictions for $l/d \to \infty$ deviate more as the "aspect ratio" l/d decreases[1] (Fig. 9).

Applying the standard aspect ratio correction for wing lift gives Eq. (16) in the following form:

$$\bar{\Omega}_{FS}/2 = (17/12)/(1 + 2d/l) \tag{17}$$

Figure 10 shows that Eq. (17) underpredicts the experimental results.[1] This is in agreement with Tarzanin's findings[11] that sudden flow separation or reattachment occurs simultaneously over part of the span of a rotating helicopter blade. A similar spanwise correlation phenomenon can be expected here, shifting the experimental results toward the two-dimensional limit. Thus, the experimental results[1] in Fig. 10 should be bounded by the predictions by Eqs. (16) and (17), as is indeed the case.

As expected, the measured maximum flat-spin rate for the cone cylinder[1,2] (Fig. 11) falls below that for the cylinder[1] (Fig. 9a). The high *Re* spin rate, occurring when the critical condition is reached at the conic end, appears to be of the same magnitude in repeated tests,[1,2] but occurs at very different Reynolds numbers. Repeat runs for the circular cylinder also show this norepeatability of the critical *Re* condition[1] (Fig. 12). Even more interesting is the fact that in one case the transition from an initial low spin rate to the maximum one occurred in combination with a reversal of the spin direction. This indicates that Reynolds number and moving-wall effects are competing with each other and with the effects of freestream turbulence and surface roughness in a manner similar to that observed for the intermittent, unsteady, asymmetric vortex shedding from slender bodies at high angles of attack.[12]

The measured effect of roughness[1,2] (Fig. 13) shows that the azimuthal location of the first trip had a significant effect. The roughness data have been added to the results shown earlier in Fig. 9. The results in Fig. 13b show that asymmetry is induced by the off-center location of the first roughness strip and consequent azimuthal movement of downstream trips, resulting in a higher flat-spin rate at subcritical Reynolds numbers than when the trip is located at the center (Figs. 13a and 13c). Of course, the trips help to produce asymmetry in all three cases. This sensitivity is in agreement with trip results for $\alpha < 90$ deg.[13] That is, the trips can increase as well as decrease the asymmetric loads. The results for the cone-cylinder-cone body[1] (Fig. 14) show this danger even more clearly. The spin rate maximum without roughness compares well with the single-cone level in Fig. 11, when one accounts for the higher

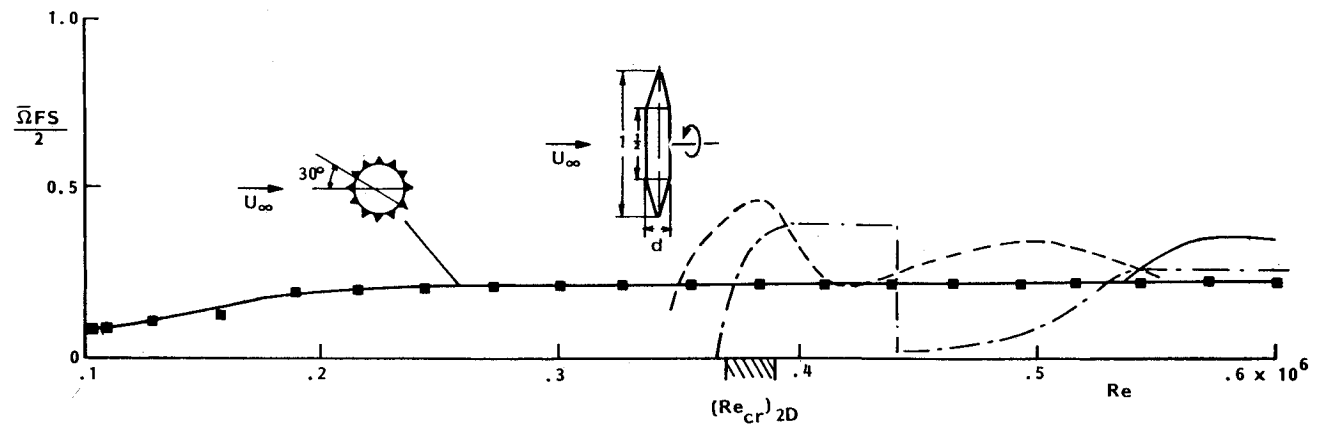

Fig. 14 Effect of boundary-layer trips on the flat-spin rate of a cone-cylinder-cone body.[1]

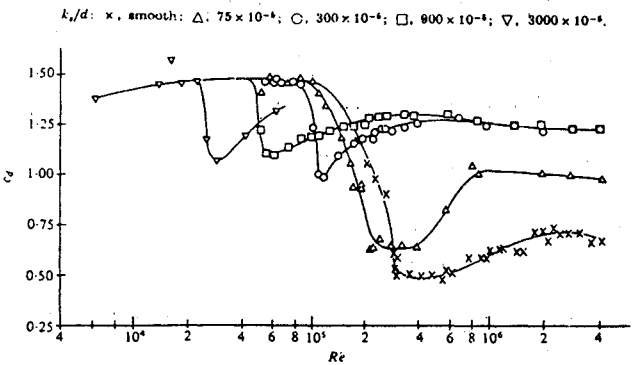

Fig. 15 Effect of roughness on circular cylinder drag.[9]

l/d, 6.09 compared to 5.5. One would expect distributed roughness to be more effective in reducing the flat-spin rate, both in regard to magnitude and Re extent. This is indicated by the 2D results for a circular cylinder[9] (Fig. 15). The diminished drag dip with increasing roughness implies that the asymmetry-induced lift Δc_ℓ will be reduced also.

Conclusions

Based upon an analysis of flat-spin characteristics of bodies with circular cross section, the following conclusions can be made:

1) Flat spin of a body with circular cross section can occur only in the critical Reynolds number region where asymmetric flow separation can be established at $\alpha = 90$ deg.

2) The boundary condition at the wall, the so-called moving-wall effect, controls the asymmetric flow separation and produces the driving moment for the flat-spin motion.

3) A simple analysis, balancing this driving moment with the drag-induced damping moment, provides predictions that bound the experimentally observed maximum flat-spin rate.

References

[1]Yoshinaga, T. and Tate, A., "Flat Spin of Slender Bodies Near the Critical Reynolds Number Region," private communication, Dec. 20, 1985.

[2]Kubota, H., Irai, I., and Matsuzaka, M., "Wind Tunnel Investigations for the Flat Spin of Slender Bodies at High Angles of Attack," *Journal of Spacecraft and Rockets*, Vol. 20, March–April 1983, pp. 108–114.

[3]Ericsson, L. E., "Flat Spin of Bodies with Circular Cross-Section," AIAA Paper 83-2147, Aug. 1983.

[4]Bearman, P. W., "On Vortex Shedding from a Circular Cylinder in the Critical Reynolds Number Regime," *Journal of Fluid Mechanics*, Vol. 37, Pt. 3, 1969, pp. 577–585.

[5]Swanson, W. M., "The Magnus Effect: A Summary of Investigations to Date," *Journal of Basic Engineering*, Vol. 83, Sept. 1961, pp. 461–470.

[6]Ericsson, L. E., "Karman Vortex Shedding and the Effect of Body Motion," *AIAA Journal*, Vol. 18, Aug. 1980, pp. 935–944.

[7]Ericsson, L. E. and Reding, J. P., "Dynamics of Forebody Flow Separation and Associated Vortices," *Journal of Aircraft*, Vol. 22, April 1985, pp. 329–335.

[8]Ericsson, L. E., "Circular Cylinder Response to Karman Vortex Shedding," AIAA Paper 86-0999-CP, May 1986; also *Journal of Aircraft* (to be published).

[9]Achenbach, E., "Influence of Surface Roughness on the Cross-Flow Around a Circular Cylinder," *Journal of Fluid Mechanics*, Vol. 46, Pt. 2, 1971, pp. 321–335.

[10]Dwyer, H. A. and McCroskey, W. J., "Crossflow and Unsteady Boundary-Layer Effects on Rotating Blades," *AIAA Journal*, Vol. 9, Aug. 1971, pp. 1498–1505.

[11]Tarzanin, F. J. Jr., "Prediction of Control Loads Due to Blade Stall," *Journal of the American Helicopter Society*, Vol. 17, April 1972, pp. 33–46.

[12]Ericsson, L. E., "Vortex Unsteadiness on Slender Bodies at High Incidence," *Journal of Spacecraft and Rockets*, Vol. 24, No. 4, July–Aug. 1987, pp. 319–325.

[13]Ericsson, L. E., and Reding, J. P., "Alleviation of Vortex-Induced Asymmetric Loads," *Journal of Spacecraft and Rockets*, Vol. 17, Nov.–Dec. 1980, pp. 548–553.